Fermilab Library
0 1160 0052545 5

SDC-90-00104

SDC
SOLENOIDAL DETECTOR NOTES

DETECTION OF ISOLATED ELECTRONS IN HEAVY HIGGS SEARCH

Hiroyuki Iwasaki

October 1990

Detection of Isolated Electrons in Heavy Higgs Search

Hiroyuki Iwasaki
KEK, *Tsukuba, Ibaraki, JAPAN*

Abstract

We studied the process $pp \to H^0 \to Z^0 Z^0 \to 4e$ for very heavy Higgs mass, M_H = 800 GeV, at $\sqrt{s}$ = 40 TeV with using PYTHIA5.3. The analysis is based entirely on a calorimetry detector. We investigated a validity of requiring just an isolated electromagnetic activity rather than positively identifying an electron. We found that such "EM-ID" is useful for this particular physics process. Also, we examined effects of "bad" regions in the calorimeter to the geometrical acceptance and the mass resolution of Z^0. The "bad" regions do not cause obvious deterioration on the mass resolution, and improve about factor two in geometrical acceptance.

1 Introduction

To uncover the mechanism of the spontaneous symmetry braking in the electroweak theory is one of the most important physics for SSC. According to the model of the minimal Higgs doublet, a physical Higgs scalar exists. Experimentally, the mass range between 32 MeV and 24 GeV is excluded recently by the ALEPH collaboration[1]. We do not know theoretically about its mass scale, except that it is less than $\sim$ 1 TeV for the perturbative approach to be valid[2]. For this purpose, we must be capable of detecting the Higgs boson up to this region.

A heavy Higgs($M_H > 2M_{W/Z}$) predominantly decay into W^+W^- or Z^0Z^0 pair. However, it is now turned out that the top-quark is expected to be heavier than the $W^\pm/Z^0$ mass[3]. Then the W^+W^- pairs can be produced copiously via $t\bar{t}$ production. Reconstruction of Z^0 through the hadronic decay mode is confronted with difficulties due to the large QCD background. The practical signal modes are therefore $H^0 \to Z^0Z^0 \to l\bar{l}\, l'\bar{l}'$, where l (l') stands for e or μ (e, μ or ν's). In this report, we will concentrate on the decay mode, $H^0 \to 4e$, and study requirements related to electron identification(e-ID).

Suppose that $\epsilon(1e)$ is the efficiency of e-ID for an electron, the detection efficiency for four electrons is $\epsilon(1e)^4$. Even the e-ID efficiency for an electron is 90%, it becomes 66% for four electrons. In fact, the CDF group reports $\sim$ 86% for $\epsilon(1e)$[4], and we do not know its value under the SSC environment with a realistic detector system. Moreover, if the Higgs mass is as heavy as 800 GeV, we need higher luminosity than 10^{33} $cm^{-2}s^{-1}$. Even with the 16 times higher luminosity, we do not gain at all if $\epsilon(1e)$ becomes factor two worse. On the other hand, the process $H^0 \rightarrow Z^0Z^0 \rightarrow 4e$ has a clean topology with the strict kinematical constraints. Therefore, we may not have to identify electrons positively, but an isolation requirement for electromagnetic activity("EM-ID") might be enough to suppress backgrounds. If it is possible, the better detection efficiency is expected, and especially so under the higher luminosity. One of the topics in this report is to investigate the capability of the "EM-ID" for this particular physics process.

The second topic is about the geometrical acceptance. A study on the requirements to e-ID for the process $H \rightarrow Z^0Z^0 \rightarrow l\bar{l}\,l'\bar{l}'$ has been done by Yamamoto *et al.*[5]. They studied the detection efficiencies of the heavy Higgs bosons by taking account of the realistic calorimeter geometry. According to the Martin-Marietta design of the liquid argon calorimeter, there are nonnegligible materials in front of the electromagnetic calorimeter at around $|\eta| \simeq 0.73$ (η is the pseudorapidity, $\eta = -\ln(\tan\theta/2)$) corresponding to the support structures and $|\eta| \simeq 1.5$ corresponding to the barrel-endcap boundaries. They abandoned to use these regions as well as the boundaries of modules in ϕ for the electron detection. If four electrons are required in the final state, the geometrical acceptance becomes less than 40%(the η-coverage of 3 is assumed). Motivated with the result, we examined effects on the geometrical acceptance and the Z^0-mass resolution when one electron was allowed to enter those kind of "bad" regions.

2 Methodology

2.1 Event generation

The process which we consider is $H^0 \rightarrow Z^0Z^0 \rightarrow 4e$, where the Higgs is produced via pp-collision at $\sqrt{s}$ = 40 TeV. The top-quark mass is assumed to be 150 GeV. As we stated before, we will concentrate our study on the very heavy Higgs, M_H = 800 GeV. We used the PYTHIA version 5.3[6] for the event generation.

The production cross section of Higgs versus its mass is plotted in Fig.1. Indeed its production rate is not necessarily small, but the branching ratio to the 4e-mode is too small($\sim 3 \times 10^{-4}$). The resulting event rate of the 4e-mode for $M_H = 800$ GeV is only 11.8 events with the integrated luminosity of $10^{40}\ cm^{-2}$. The mass distribution, the rapidity (y_H) distribution, and the the transverse momentum (p_T) distribution are shown in Fig.2a, Fig.2b and Fig.2c, respectively. We generated 1000 events for this process. Since the decay width of the Higgs boson is proportional to M_H^3, it becomes about 300 GeV for $M_H = 800$ GeV (Fig.2a). Since it is heavy, it is produced in the central region, $|y_H| < 2$ (Fig.2b). As for the transverse momentum, it has the large tail (Fig.2c). As the result, the Z^0 bosons are not necessarily produced in the back-to-back configuration. In Fig.2d, the acoplanarity angle between the two Z^0 bosons is shown. We should note that the jet activity is not small even in this type of "clean" physics process.

2.2 Detector

The detector used in this analysis is a calorimeter system only. It covers up to $|\eta| = 3$ and has the tower geometry with the tower size $\Delta\eta \times \Delta\phi = 0.05 \times 0.05$. Each tower is longitudinally segmented into two parts, an electromagnetic section(EM) and a hadronic one(HAD). The energy resolutions of the electromagnetic and hadronic sections are $\sigma_E/E = 0.2/\sqrt{E} + 0.02$ and $0.5/\sqrt{E} + 0.02$, respectively, where E is the deposited energy in the tower in GeV. The angular resolutions are $\sigma_\eta = \sigma_\phi = 2.5 \times 10^{-3}$, which corresponds to the position resolution of $\sigma_x = 5mm$ at $2m$ away from the interaction point at $\eta = 0$. Worse energy and angular resolutions are used in some "bad" regions as explained in the followings.

Fig.3a shows a quadrant side view of a liquid argon calorimeter with a coil inside designed by the KEK group[7,8]. In Fig.3b, the materials in front of the EM section in radiation length(X_0) is plotted as a function of pseudorapidity[1][9]. The blank area is due to the magnet, and the shaded area is due to the vessel walls of the calorimeter. The thickness is about $2\,X_0$ at $\eta = 0$, and gradually increases up to $4\,X_0$ at $\eta \simeq 1.4$. At $\eta \simeq 1.5$, the thickness becomes $\sim 6\ X_0$. In Fig.4, we plot the energy resolution versus the material thickness in front of the calorimeter calculated by using the EGS simulation[10]. Without any correction(filled circle), the resolution becomes considerably worse beyond $X_0 > 2$. However, by using the "massless-gap method"(open circle), where some absorber plates are removed

[1]Since the calorimeter design is revised frequently, the figure should be taken so.

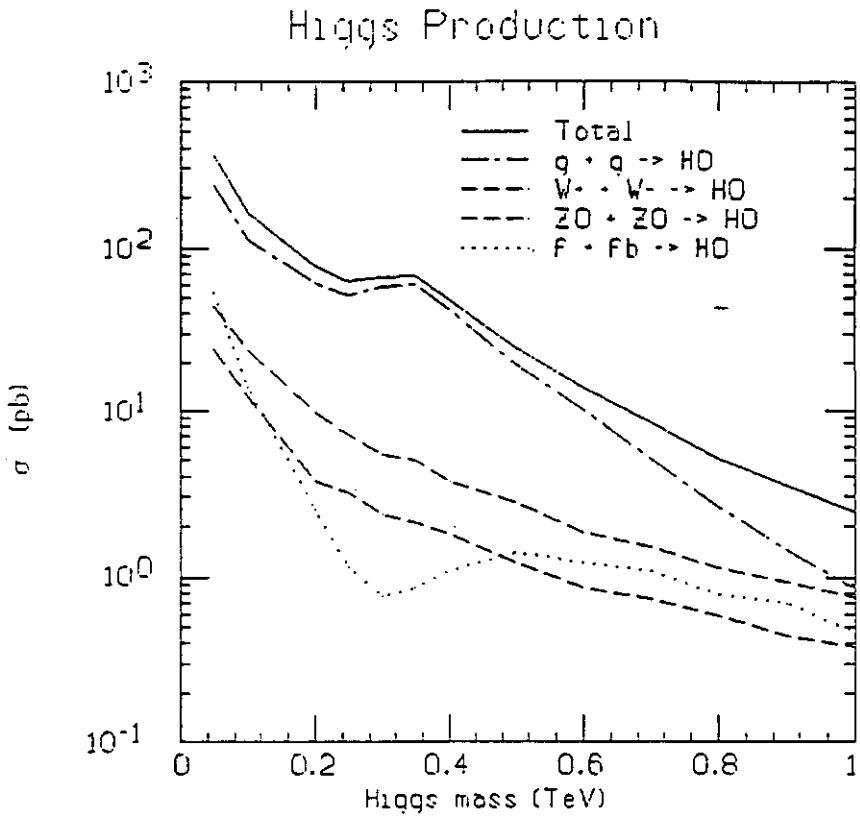

Fig.1. The Higgs production cross section versus its mass via pp-collision at $\sqrt{s}$ = 40 TeV calculated by using PYTHIA version 5.3[6]. The top-quark mass is assumed to be 150 GeV.

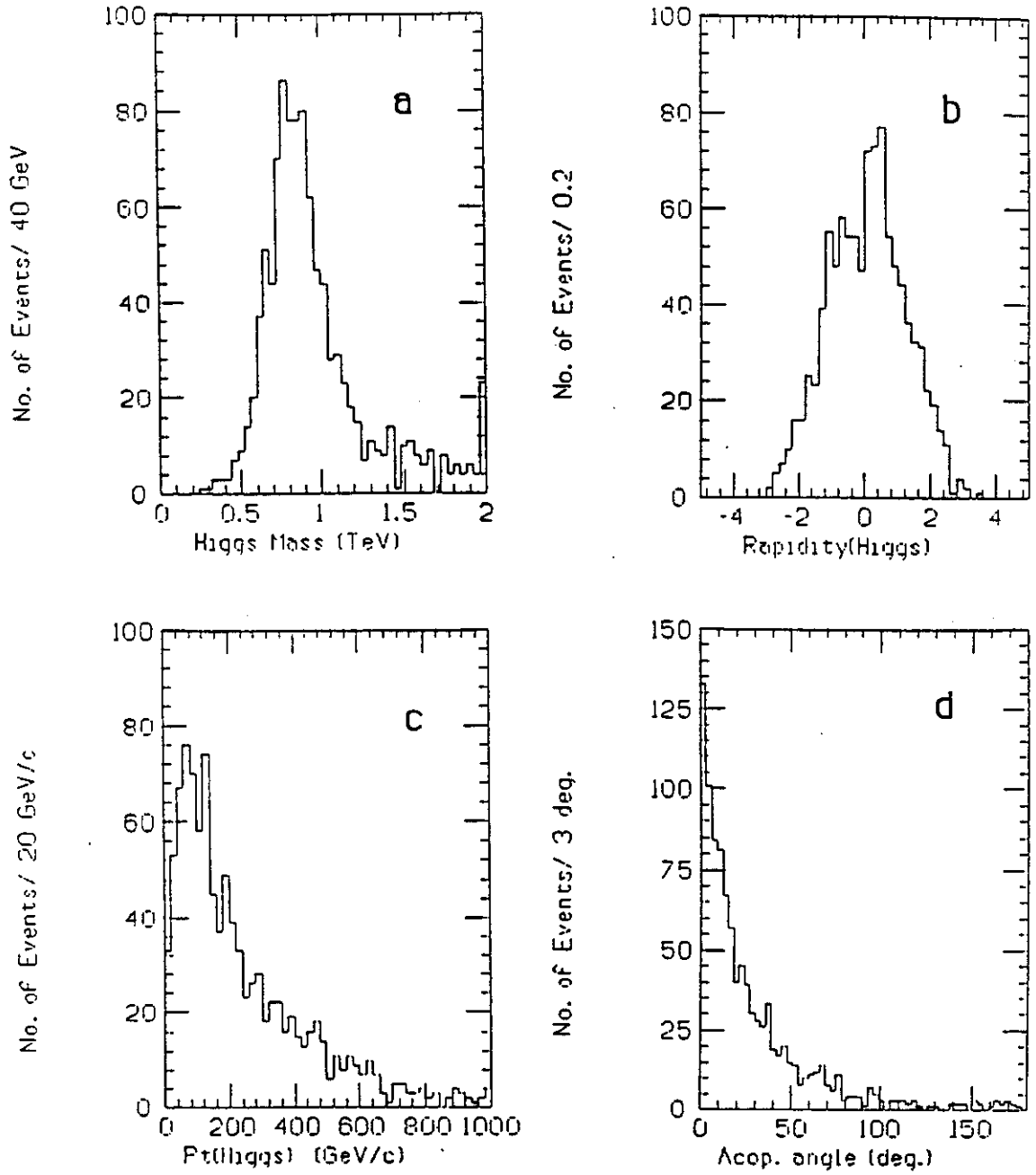

Fig.2. (a) The mass distribution of the Higgs boson at $M_{H} = 0.8$ TeV. (b) Its rapidity distribution. (c) Its transverse momentum(P_T) distribution. (d) The acoplanarity angle between the two Z^0 bosons which are the decay products of the Higgs boson.

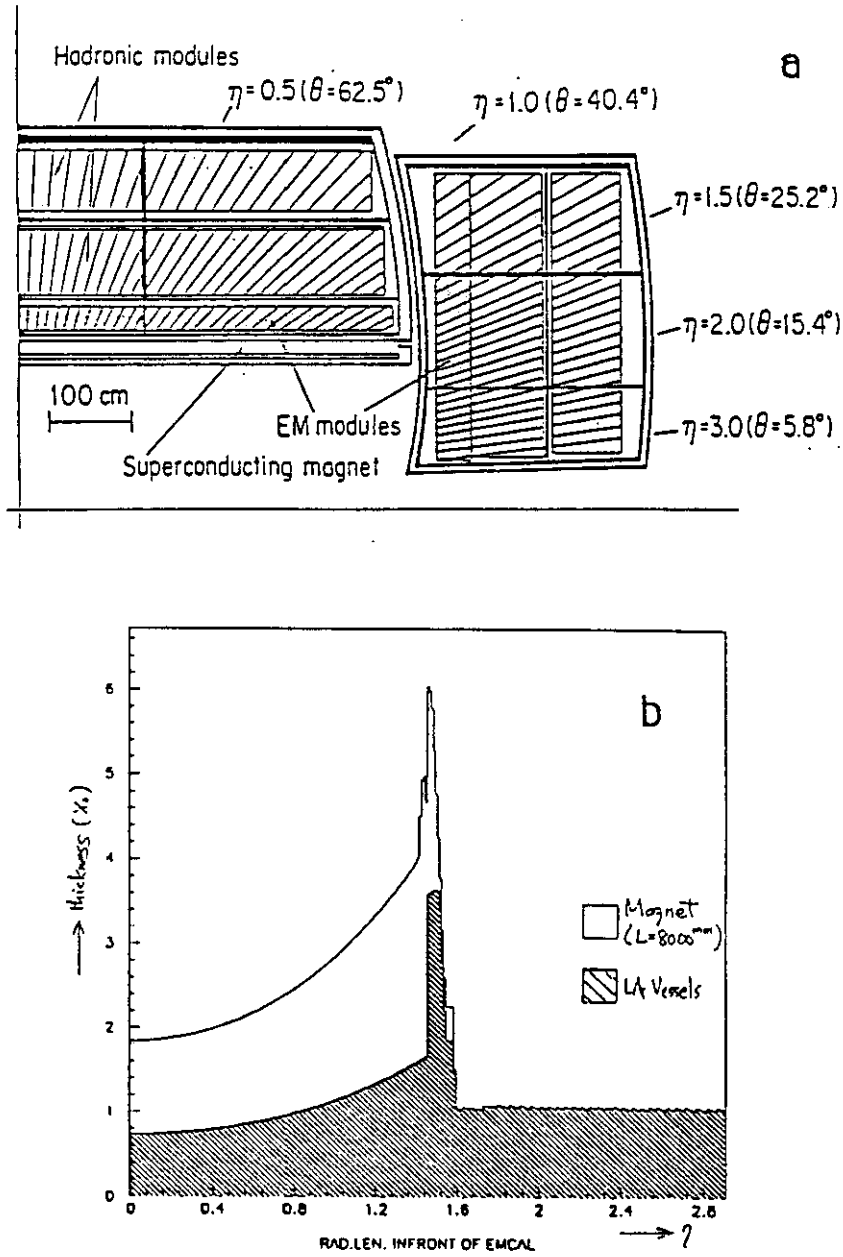

Fig.3. (a) A quadrant side view of a liquid argon calorimeter with a coil inside[7,8]. (b) The materials in front of the electromagnetic section in radiation length(X_0) versus pseudorapidity[9]. The blank area is due to the coil, and the shaded area is due to the vessel walls of the calorimeter.

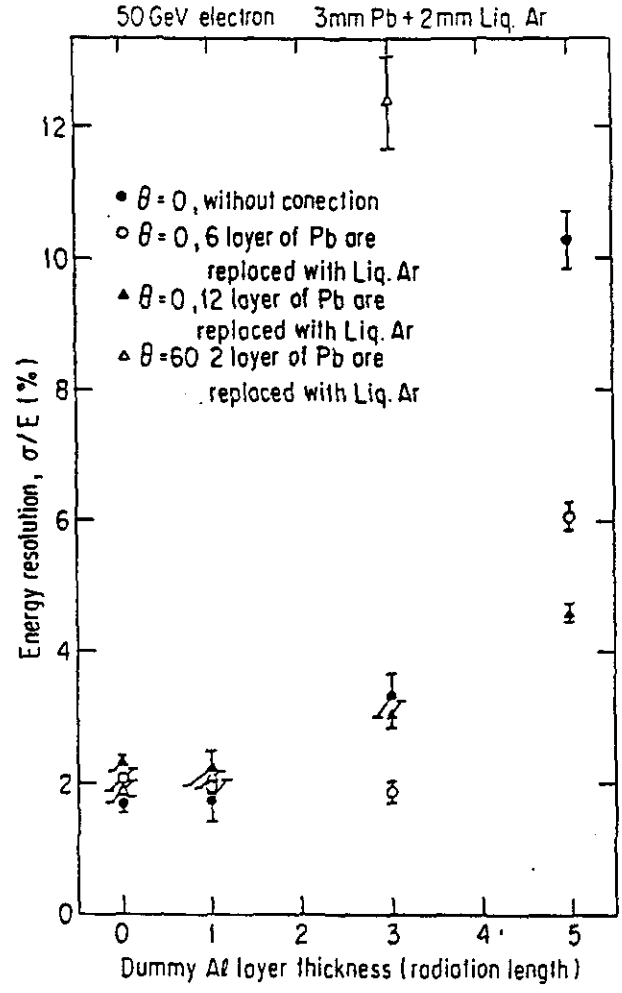

Fig.4. The energy resolution versus the material thickness in front of the electromagnetic calorimeter calculated by using the EGS simulation[10].

Table 1. Resolution parameters of the EM calorimeter

η	A ($\sigma_E/E = A/\sqrt{E} + 0.02$) "good" in ϕ	"bad" in ϕ	$\sigma_\eta = \sigma_\phi$
"good" in η	0.2	0.4	2.5×10^{-3}
$1.1 < \lvert\eta\rvert < 1.4$	0.3	0.5	5.0×10^{-3}
$1.4 < \lvert\eta\rvert < 1.55$	0.6	0.8	1.0×10^{-2}

but the shower sampling is kept working, the resolution becomes the same level up to $X_0 \simeq 3$ as that at $X_0 = 0$. Thus, we define the "bad" region in η where the thickness is larger than $3X_0$, namely $1.1 < \eta < 1.55$.

We assume "bad" tower-rows every 16 tower-rows in ϕ, which corresponds to about $6mm$ "bad" boundary region between the two adjacent towers if the EM section is placed at $2m$ away from the beam line. The energy resolutions and the angular resolutions in the "bad" regions are summarized in Table1. Since the position resolution is better for an electron hitting the tower boundary, we assume the angular resolutions are independent of ϕ.

2.3 Event analysis

In the energy deposition in a tower, we assume that all the electromagnetic(hadronic) energy is deposited only in the electromagnetic(hadronic) section, and that there is no correlation between the two sections. Deposited energy in a tower is smeared independently for electromagnetic activity and hadronic one. The transverse sharing of shower energy between towers is also neglected.

For each electron, which are decay product of a Higgs boson, its hit position is smeared. The electromagnetic energies in all the towers inside the window of ± 1 in η and ϕ (3×3 towers) around the tower where the electron hits are merged($\equiv E^{EM}(3 \times 3)$). For the hadronic activity with respect to the electron, it is defined as an energy sum inside the window of ± 3 in η and ϕ (7×7 towers) for all the particles except $e^{\pm}$, $\mu^{\pm}$, and ν's ($\equiv E^{HAD}(7 \times 7)$). The same merging procedure is also applied to γ or $e^{\pm}$, which is not the decay product of the Higgs boson, if its E_T in a seed tower is larger than 5 GeV. These clusters are referred to as fake clusters.

Selection requirements

Event selection criteria are the followings.

1. $|\eta|$ is less than 2.8 for all the four electrons.

2. Number of electrons which enter the good regions, N_{good}, is 3 or 4.

3. Transverse energy, $E_T^{EM}(3 \times 3)$, is larger than 20 GeV for all the four electrons.

4. For each electron, the ratio of hadronic activity to that of the electron, HAD/EM, is less than 0.1:

$$HAD/EM \equiv \frac{E_T^{HAD}(7 \times 7)}{E_T^{EM}(3 \times 3)} < 0.1.$$

5. We select a combination of electron pairs in such a way to minimize the quantity,

$$(M(e_1e_2) - M_Z)^2 + (M(e_3e_4) - M_Z)^2.$$

6. The mass difference, $|M(e_ie_j) - M_Z|$, is less than 10 GeV for both the Z^0 candidates.

3 Results

3.1 Detection efficiency and mass resolution

3.1.1 Geometrical cuts

Fig.5a shows the pseudorapidity distribution of electrons which are the decay products of the Higgs boson. More than 80% of the electrons enter within $|\eta| = 2$. However, if all the four electrons are to be detected, the detector coverage should be up to $|\eta| \simeq 3$. Fig.5b shows the distribution of the maximum pseudorapidity out of the four electrons in an event, $|\eta|_{max}$. If we require $|\eta|_{max} < 2.8$, 86% of the events survive.

N_{good} (defined in section 2.3) distribution for those events which satisfy $|\eta|_{max} < 2.8$ is shown in Fig.6. If we require all the electrons to enter the "good" regions, only about 40% of the events remain. However, if we can allow one electron to enter the "bad" regions, we gain other 40% of the events. As we will see later, it is really the case. The resulting detection efficiency due to the geometrical cuts becomes 77%.

3.1.2 Physics cuts and mass resolutions

Fig.7 shows the minimum transverse energy of the electrons in an event , $E_T^{EM}(3 \times 3)_{min}$, after the geometrical cuts. If we require $E_T^{EM}(3 \times 3)_{min}$ to be larger than 20 GeV, 96% of the events survive. The measure of the isolation, HAD/EM, is plotted in Fig.8a for the signal electrons which satisfy $E_T^{EM}(3 \times 3) > 20$ GeV. It has

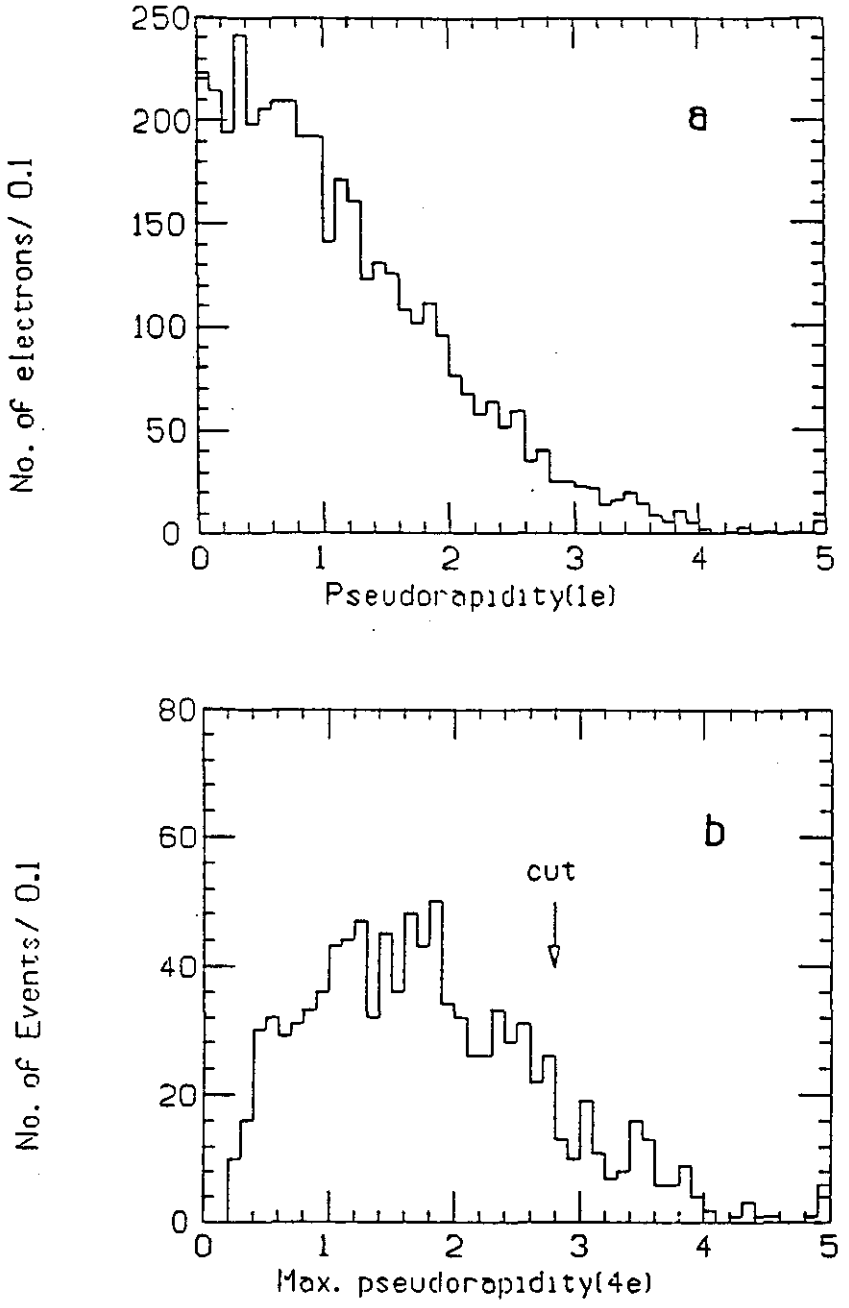

Fig.5. (a) The pseudorapidity distribution of each electron which is a decay product of the Higgs boson. (b) The distribution of the maximum pseudorapidity out of the four electrons in an event.

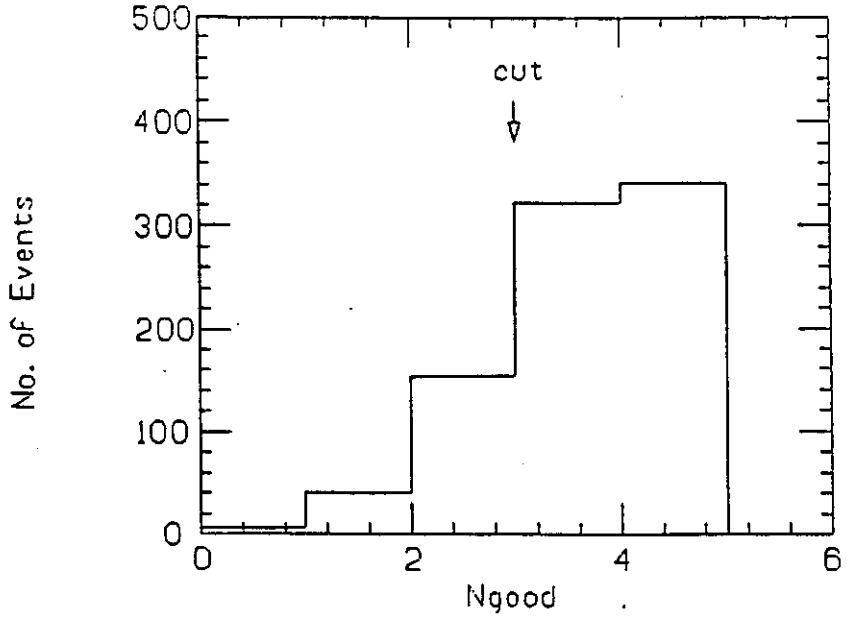

Fig.6. N_{good} (defined in section 2.3) distribution for those events where $|\eta|_{max} < 2.8$ is satisfied.

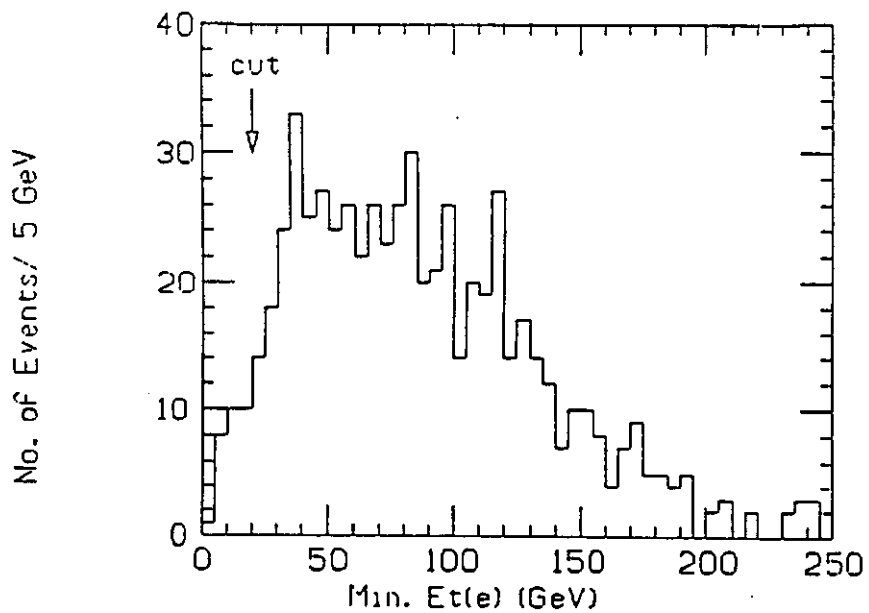

Fig.7. The minimum transverse energy of the electrons in an event after the geometrical cuts.

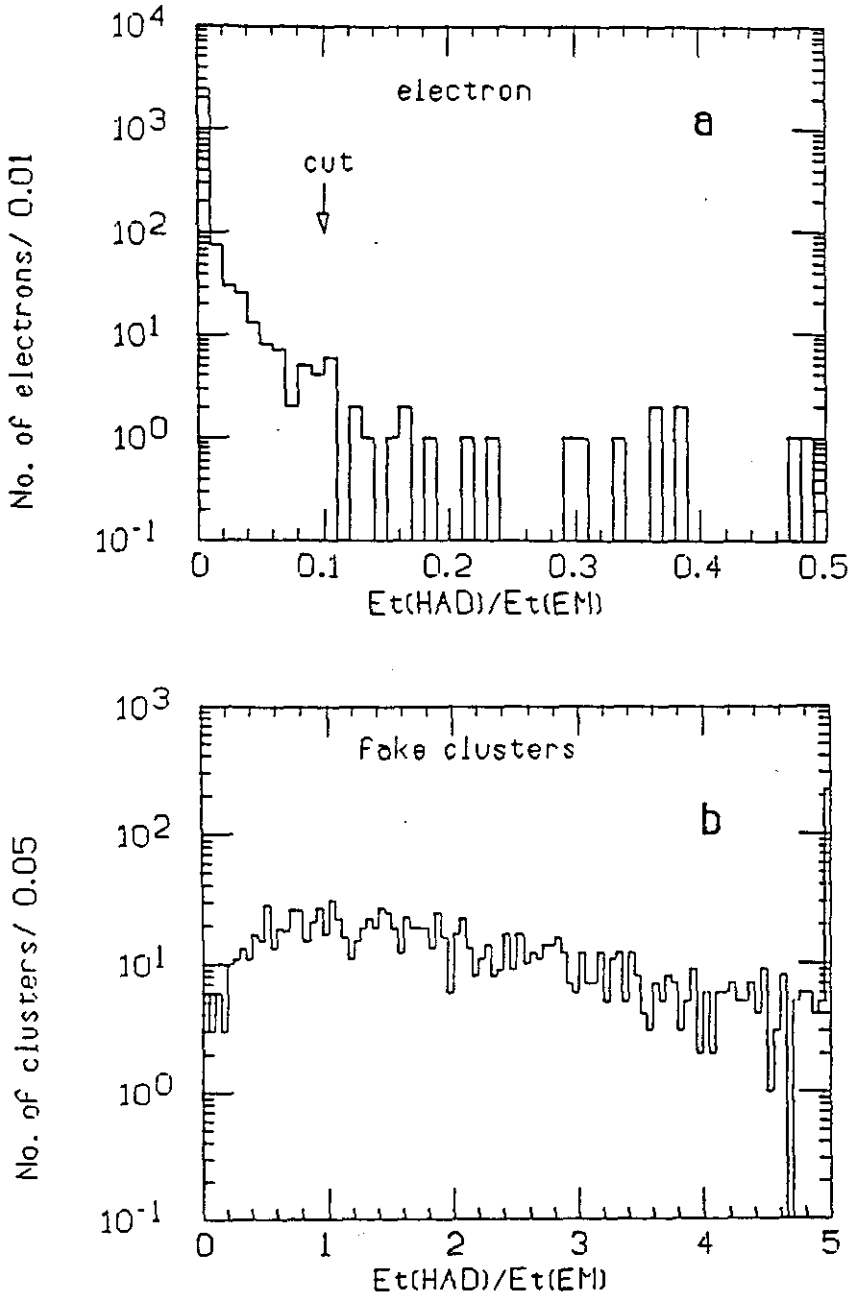

Fig.8. (a) The measure of the isolation, HAD/EM, for the signal electrons which satisfy $E_T^{EM}(3\times3) > 20$ GeV/c. (b) The distribution for fake clusters which satisfy $E_T^{EM}(3 \times 3) > 20$ GeV/c in the same process, $pp \rightarrow H^0 \rightarrow 4e$.

a sharp peak at $HAD/EM \simeq 0$, and 99% of the electrons satisfy the requirement, $HAD/EM < 0.1$. Being required for all the four electrons in an event to satisfy the isolation condition, 96% of the events remain.

After the geometrical cuts and the isolation cut, we select a combination of electron pairs, for which the quantity, $(M(e_1e_2) - M_Z)^2 + (M(e_3e_4) - M_Z)^2$, is the smallest. There is no wrong combination out of 610 events. Fig.9a shows the invariant mass distribution of the electron pair where both of them enter the "good" regions after the $E_T^{EM}(3 \times 3)_{min}$ and the HAD/EM cuts. Fig.9b shows the similar distribution, but one of the electrons enters the "bad" regions. There is no obvious difference between the two distributions [2]. If we require both the Z^0 candidates to satisfy the condition, $|M(ee) - M_Z| < 10$ GeV, 92% of the events survive.

Invariant mass distribution of four electrons, $M(ZZ)$, after all the physics cuts is plotted in Fig.10. The broad peak is simply due to its natural width(see Fig.2a) Contribution from the detector resolution is negligible. If we select the region, 600 GeV $< M(ZZ) <$ 1200 GeV, 78% of the events survive. In Table 2, we summarize the requirements, the efficiencies, and the number of events after the each requirement step with the nominal integrated luminosity for one experimental year, $10^4\,\mathrm{pb}^{-1}$.

3.2 Answers to the questions

3.2.1 Do we really need e-ID?

The HAD/EM distribution for the fake clusters in the same process, $pp \to H^0 \to 4e$, is shown in Fig.8b. Note that the horizontal scale is different from Fig.8a. After the isolation cut, 0.9×10^{-2} clusters per event remain. Since we apply only "EM-ID", these fake clusters are considered as electrons. Taking account of this rate and the probability to choose a wrong combination of electron pairs($< 2 \times 10^{-3}$), we do not have to identify electrons positively, but just to require isolated EM-clusters as long as the signal events are concerned. As we will see in the next section, the "EM-ID" is enough to suppress the backgrounds to negligible level. The only exception is the continuum Z^0Z^0 production, where application of the positive e-ID dose not help further than the "EM-ID". Thus, we may conclude

[2] As a check, we plot the $M(ee)$-distribution in Fig.9c similar to Fig.9b, but with the twice worse resolution in the "bad" regions for both energy and angular measurements. In this case the difference from Fig.9a is obvious

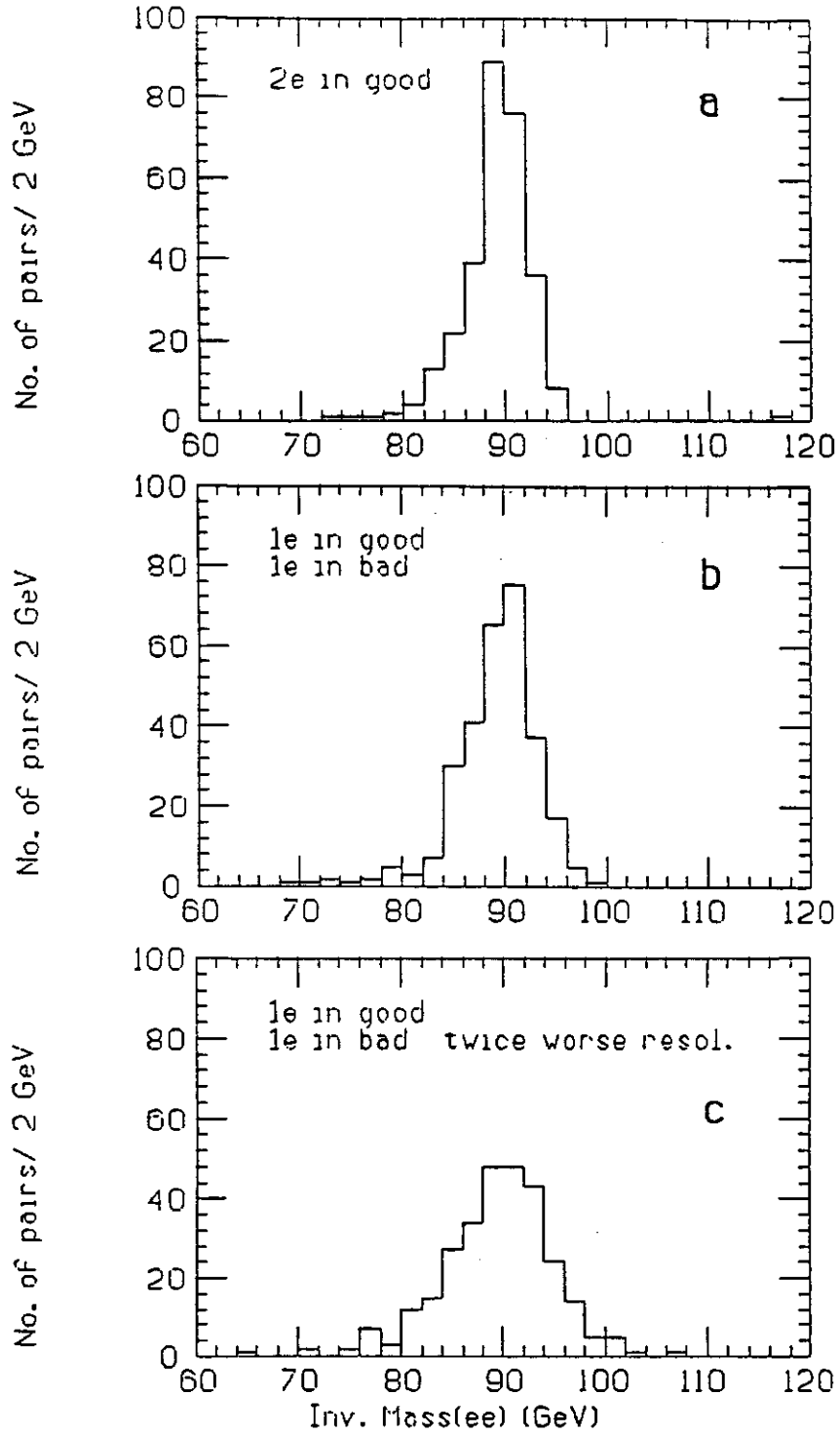

Fig.9. (a) The invariant mass distribution of the electron pair where both of them enter the "good" regions after the $E_T^{EM}(3\times 3)$ and the HAD/EM cuts. (b) Similar distribution as (a), but one of the electrons enter the "bad" regions. (c) Similar distribution as (b), but with the twice worse resolution in the "bad" regions for both energy and angular measurements.

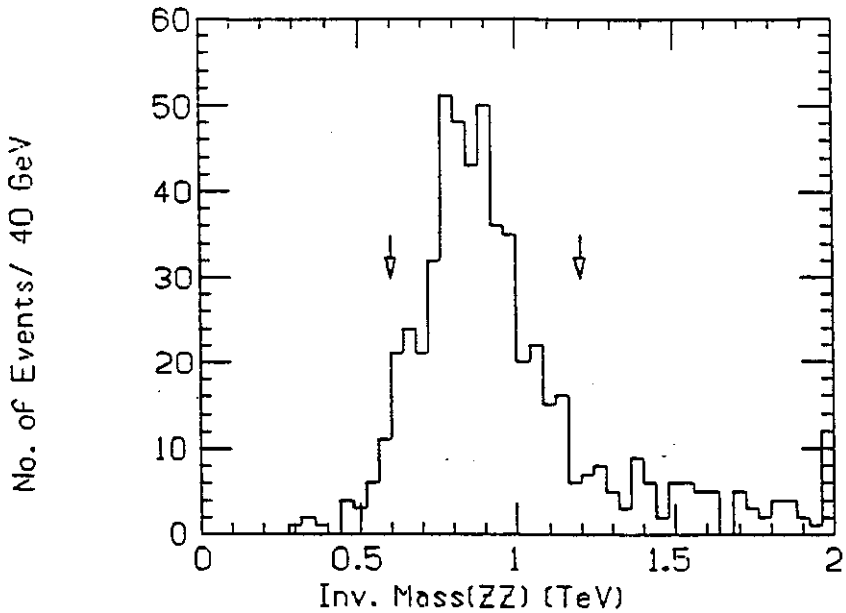

Fig.10. The invariant mass distribution of the four electrons, $M(ZZ)$, after the physics cuts.

Table 2. Efficiencies and the number of events per year

	$H^0 \to 4e$		$Z^0Z^0 \to 4e$ (continuum)	
Cross section	1.18×10^{-3} pb		3.49×10^{-3} pb	
selection	effic.	Evts/ yr.	effic.	Evts/ yr.
without cuts		11.8		34.9
$\|\eta\|_{max} < 2.8$	0.86	10.2	0.41	14.5
$N_{good} = 3, 4$	0.77	7.8	0.79	11.5
$E_T^{EM} > 20$ GeV	0.96	7.5	0.65	7.5
HAD/EM	0.96	7.2	0.98	7.3
$\|\Delta M_Z\| < 10$ GeV	0.92	6.6	1.00	7.3
$0.6 < M_H < 1.2$ TeV	0.78	5.2	0.24	1.8
overall	0.44	5.2	0.05	1.8

One experimental year corresponds to $10^4 pb^{-1}$.

that the requirement of isolated electromagnetic activity is enough for the heavy Higgs search in the process, $pp \to H^0 \to 4e$.

3.2.2 De we have to abandon the "bad" regions?

As we see in the previous subsection, the mass resolution of Z^0 with one "bad" electron is almost the same as that with two "good" electrons. If the assumption for the energy resolutions and the angular resolutions is not so far away from the reality, we can use the "bad" regions with keeping good quality in mass resolution. By just allowing one electron may enter the "bad" regions, the geometrical acceptance becomes about twice larger.

4 Background study

4.1 $q\bar{q} \to Z^0 Z^0 \to 4e$ (continuum)

The cross section is 3.5×10^{-3} pb for $\sqrt{\hat{s}} > 400$ GeV, where $\sqrt{\hat{s}}$ is the cm energy in the $q\bar{q}$ system. It is about three times larger than that of the Higgs production, $H^0 \to 4e$, at $M_H = 800$ GeV. We generated 3000 events for this process. The $|\eta|_{max}$ distribution, the $E_T(3 \times 3)_{min}$ distribution, and the $M(ZZ)$ distribution are plotted in Fig.11, Fig.12, and Fig.13, respectively. Other distributions are similar to those for signal events. About 41% of the events enter the region, $|\eta|_{max} < 2.8$. The requirement of $E_T(3 \times 3)_{min} > 20$ GeV rejects 35% of the events after the geometrical cut. As for the $M(ZZ)$ distribution, 24% of events enter the signal region, 600 GeV $< M(ZZ) <$ 1200 GeV. The resulting overall detection efficiency is 5%, which is to be compared with 44% for the signal. The detection efficiencies and the number of events at each step are also summarized in Table 2

4.2 $pp \to Z^0 + jet \to 2e + jet$

The cross section is 30.7 pb for $\sqrt{\hat{s}} > 400$ GeV and $p_T > 100$ GeV. It is 2.6×10^4 times larger than the signal process, $H^0 \to 4e$. We generated 10000 events for this process. In Fig.14, we show the HAD/EM distribution for those clusters (except the electrons from Z^0) which satisfy $|\eta| < 2.8$ for the seed tower, and $E_T^{EM}(3 \times 3) >$ 20 GeV. Since our requirement for an electron is just the HAD/EM value should be less than 0.1, the rate to misidentify the fake cluster as an electron is 0.7×10^{-2}

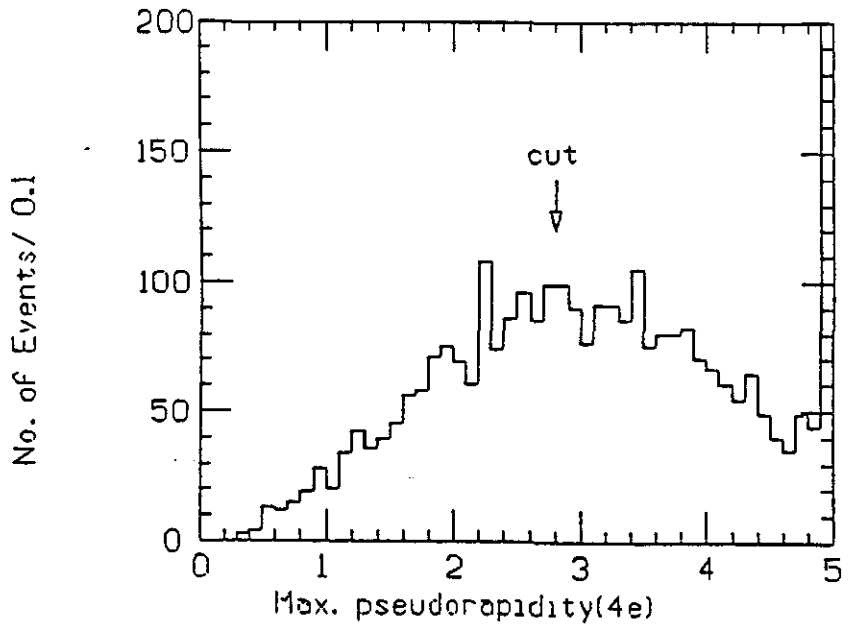

Fig.11. The $|\eta|_{max}$ distribution for the continuum process, $q\bar{q} \to Z^0 Z^0 \to 4e$.

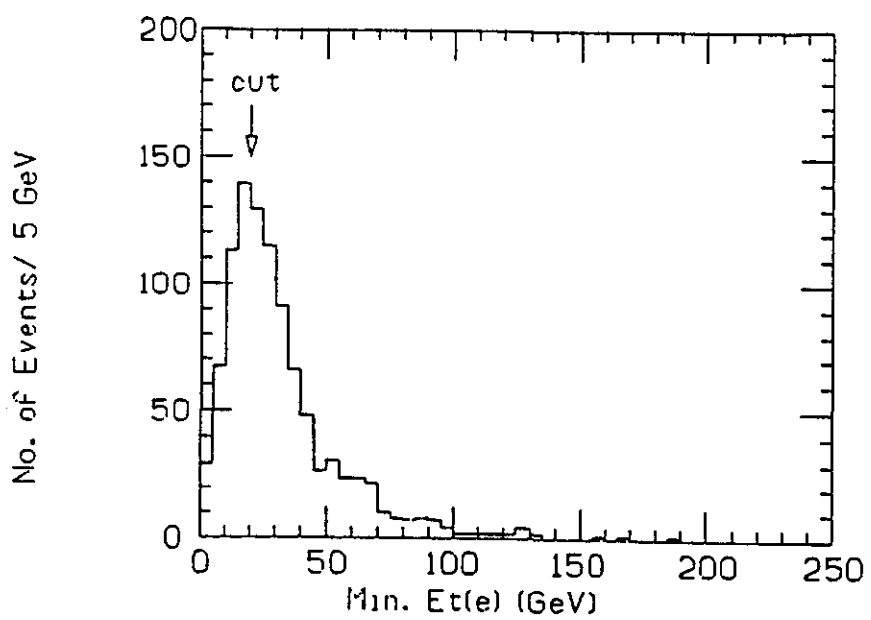

Fig.12. The $E_T^{EM}(3 \times 3)_{min}$ distribution for the continuum process, $q\bar{q} \to Z^0 Z^0 \to 4e$.

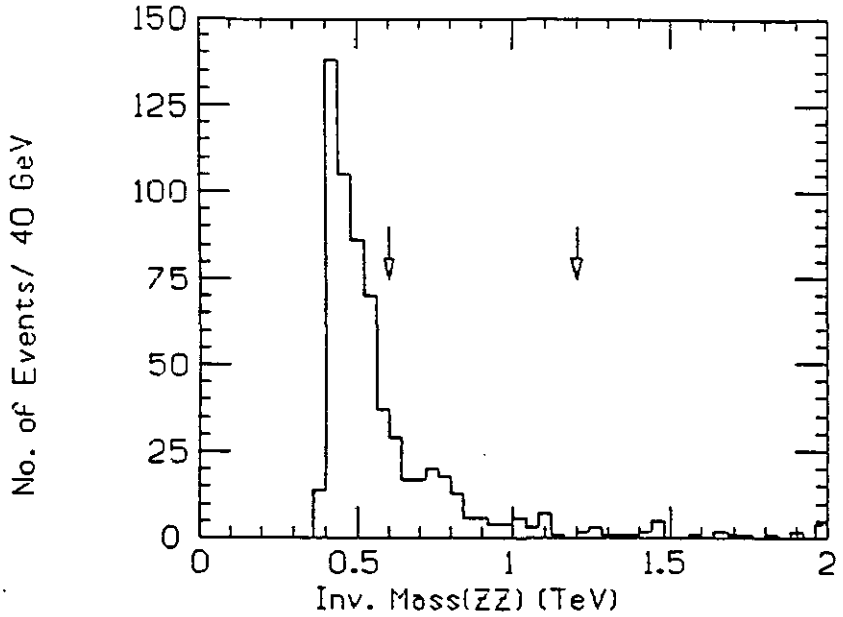

Fig.13. The invariant mass distribution of the four electrons for the continuum process, $q\bar{q} \rightarrow Z^0 Z^0 \rightarrow 4e$.

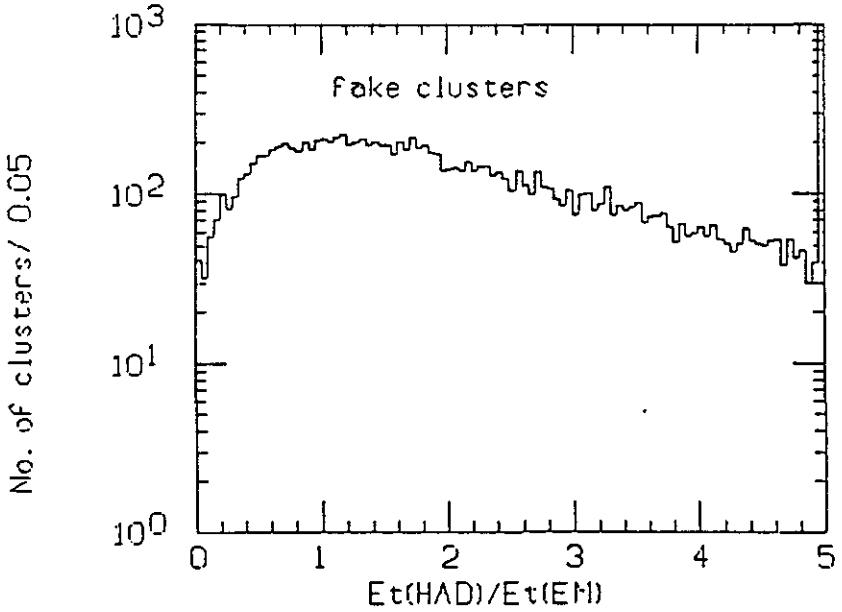

Fig.14. The HAD/EM distribution for those clusters which satisfy $|\eta| < 2.8$ for the seed tower, and $E_T^{EM}(3 \times 3) > 20$ GeV for the process, $pp \rightarrow Z^0 + jet \rightarrow 2e + jet$.

clusters per event. Therefore, the probability to find two such fake clusters in an event is about 5×10^{-5}. We need millions of events, if we straightforwardly estimate the probability to misidentify the "electron" pair as Z^0. Instead, we could estimate the probability using the same cluster sample without imposing the isolation requirement, $HAD/EM < 0.1$. In Fig.15, we plot the invariant mass distribution of the cluster pair for which the distance between the two clusters, $\Delta R(= \sqrt{(\Delta\eta)^2 + (\Delta\phi)^2})$, is larger than 0.2. From the figure, we estimate the probability that the pair is consistent with Z^0 to be about 10%. The invariant mass distribution of the real Z^0 and the fake Z^0, $M(Z"Z")$, is plotted in Fig.16. The probability to fake the Higgs boson, 600 GeV $< M(Z"Z") <$ 1200 GeV, is less than 2×10^{-3}. The resulting overall probability to fake Higgs signal for the current process is estimated to be less than $\sim 1 \times 10^{-8}$. It corresponds to the cross section of 3.1×10^{-7} pb, which should be compared to 5.2×10^{-4} pb ($= \sigma(H^0 \to 4e) \times 44\%$) for signal. Although the estimation is rather crude, this background would be negligible.

4.3 Other backgrounds

4.3.1 $q\bar{q} \to Z^0\gamma g$ / $gq(/\bar{q}) \to Z^0\gamma q(/\bar{q})$

The cross sections for these processes would be roughly about order $O(\alpha)$ smaller than that of $pp \to Z^0 jet$, where α is the fine structure constant. Since we do not positively require the electron identification in the present study, we inevitably consider the photon as an electron. The probability to find a fake cluster in an jet (or jets) per event, $\varepsilon(j \to "e")$, is order of $\sim 1 \times 10^{-2}$, which is the same order of α. Therefore, the overall background level of these processes are estimated to be the same order as that of $pp \to Z^0 jet$, and are therefore negligible.

$$Bkgd(Z^0\gamma j) \simeq Bkgd(Z^0 j)\frac{O(\alpha)}{\varepsilon(j \to "e")} \simeq Bkgd(Z^0 j)$$

4.3.2 $q\bar{q} \to Z^0\gamma\gamma$

Since the cross section for $pp \to Z^0\gamma$ is almost the same for $pp \to Z^0Z^0$ at $\sqrt{s} =$ 40 TeV[11], we could estimate the cross section for $pp \to Z^0 2\gamma \to 2e2\gamma$ as

$$\frac{\sigma(pp \to Z2\gamma \to 2e2\gamma)}{\sigma(pp \to ZZ \to 4e)} \simeq \frac{\sigma(pp \to Z\gamma)\, O(\alpha)}{\sigma(pp \to ZZ)\, Br(Z \to 2e)} \simeq \frac{1}{4},$$

where $Br(Z^0 \to 2e)$ is the branching ratio of the decay mode $Z^0 \to e^-e^+$. Moreover, the probability for the γ pair to be consistent with the Z^0 mass, $\varepsilon(2\gamma \to "Z")$,

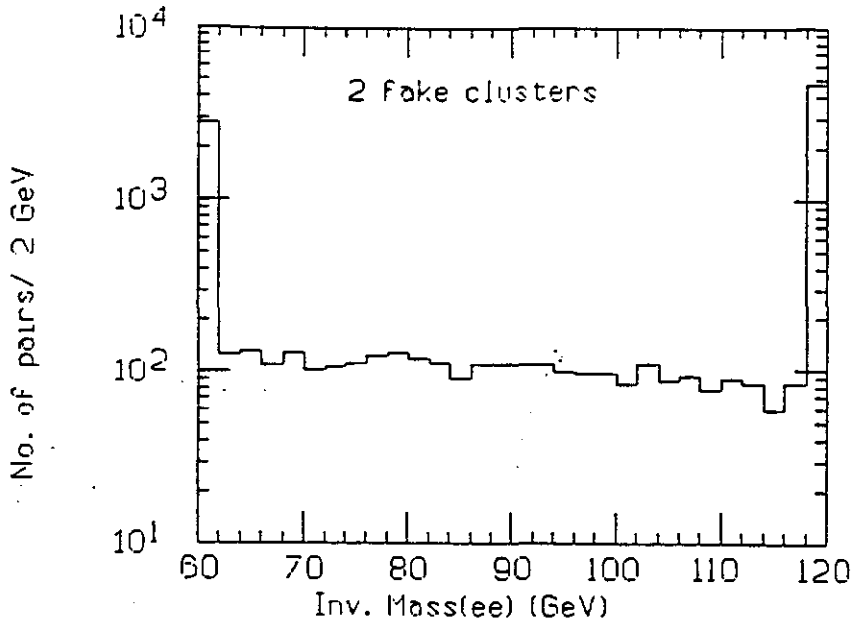

Fig.15. The invariant mass distribution of the fake cluster pair, $M(\text{"}e\text{"}\text{"}e\text{"})$, for which the distance between the two cluster, ΔR, is larger than 0.2 for the process, $pp \to Z^0 + jet \to 2e + jet$.

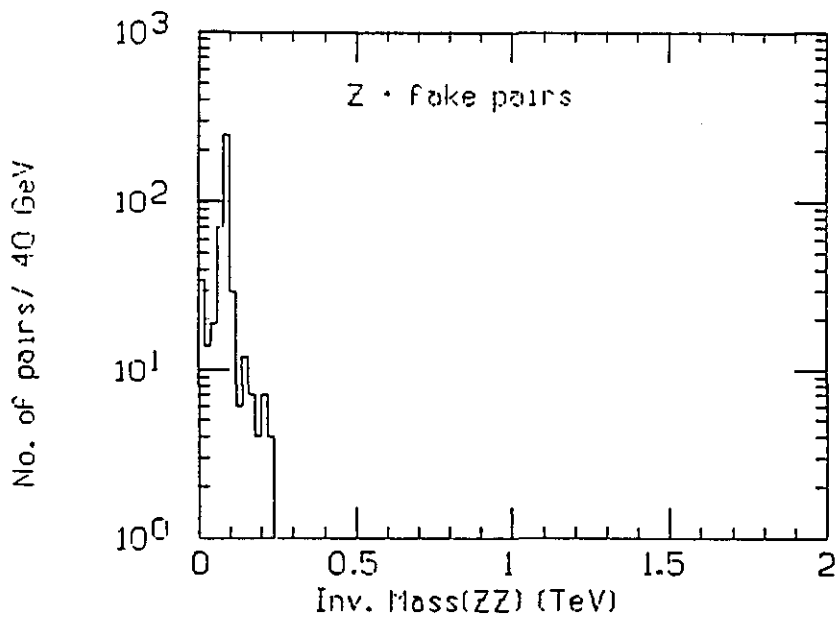

Fig.16. The invariant mass distribution of the real Z^0 and the fake Z^0, $M(Z\text{"}Z\text{"})$, for the process, $pp \to Z^0 + jet \to 2e + jet$.

is expected to be at most oder of $\sim 10\%$. Thus this process would be negligible compared to the continuum process, $pp \to ZZ \to 4e$.

$$Bkgd(Z^0\gamma\gamma) \simeq Bkgd(Z^0Z^0)\frac{1}{4}\epsilon(2\gamma \to \text{"}Z\text{"}) \ll Bkgd(Z^0Z^0)$$

4.3.3 $q\bar{q} \to \gamma\gamma\gamma\gamma$

With the similar argument as in the previous section, this background level is estimated as

$$Bkgd(\gamma\gamma\gamma\gamma) \simeq Bkgd(Z^0\gamma\gamma)\frac{O(\alpha)\,\epsilon(2\gamma \to \text{"}Z\text{"})}{Br(Z \to 2e)} \ll Bkgd(Z^0\gamma\gamma)$$

Thus, this process is further smaller than the process $q\bar{q} \to Z^0\gamma\gamma$, and is negligible.

4.3.4 $q\bar{q} \to \gamma\gamma\gamma g \;\; / \;\; gq(/\bar{q}) \to \gamma\gamma\gamma q(/\bar{q})$

With the similar argument as in section 4.3.1, this background level is estimated as

$$Bkgd(\gamma\gamma\gamma g) \simeq Bkgd(\gamma\gamma\gamma\gamma)\frac{O(\alpha_s)}{O(\alpha)}\epsilon(j \to \text{"}e\text{"}) < Bkgd(\gamma\gamma\gamma\gamma),$$

where α_s is the strong coupling constant. Therefore, this process is also negligible.

5 Summary

We studied the process $pp \to H^0 \to Z^0Z^0 \to 4e$ for very heavy Higgs mass, $M_H = 800$ GeV, at $\sqrt{s} = 40$ TeV with using PYTHIA5.3. The analysis was based entirely on the calorimetry detector. We took account of the "bad" regions in the calorimeter system at the barrel-endcap boundaries and the module boundaries.

If we use only the "good" regions and apply positive e-ID, the efficiency becomes only about 15 %. Since the cross section itself is small, we have to save signal events as much as possible with keeping good signal-to-background ratio. For this purpose, we investigated the validity of "EM-ID" instead of e-ID and examined effects of the "bad" regions to the acceptance and the mass resolution of Z^0.

As for the first subject, the isolation requirement on electromagnetic activities is enough for this particular physics process. The main background is the continuum Z^0Z^0 production, where the positive e-ID does not help to suppress further. The signal-to-background ratio is about 3. Other backgrounds such as

$Z^0 + jet$, $Z^0 + jet + \gamma$, and $Z^0 + \gamma + \gamma$, are estimated to be negligible. As for the second subject, the "bad" regions do not cause obvious deterioration on the mass resolution of Z^0, and improve about factor two in geometrical acceptance.

Even with the contrivances to loosen the e-ID and to use the "bad" regions, the overall detection efficiency is about 45 %. Since the cross section is too small for the very heavy Higgs boson, we need much higher luminosity than $10^{33}\ cm^{-2}s^{-1}$. Under such environment, the "EM-ID" would be much effective in the detection efficiency than the positive e-ID.

References

[1] ALEPH Collab., D. Decamp et al., Phys. Lett. B 236 (1990) 233; Phys. Lett. B 241 (1990) 141.

[2] B. W. Lee, C. Quigg, and H. B. Thacker, Phys. Rev. Lett. 38 (1977) 883; Phys. Rev. D 16 (1977) 1519.

[3] CDF Collab., F. Abe et al., Phys. Rev. Lett 64 (1990) 142. P. J. Franzini, Phys. Rep. 173 (1989) 1.

[4] S. Kim, talk in this Workshop.

[5] H. Yamamoto, Solenoidal Detector Notes, SSC-SDE-9 (Aug. 1989); J. Bensinger, H. Yamamoto, and E. M. Wang, talk presented at ANL Workshop (Nov. 16-18, 1989).

[6] H. -U. Bengtsson and T. Sjöstrand, "PYTHIA: The Lund Monte Carlo for Hadronic Processes",*Proc. of the 1986 Summer Study on the Physics of the Superconducting Supercollider*, ed. R. Donaldson and J. Marx, Snowmass, Colorado, 1986, p. 311.

[7] Y. Unno, talk in the calorimeter session of this Workshop.

[8] A. Yamamoto, talk in this Workshop.

[9] M. Asai, talk in the calorimeter session of this Workshop.

[10] H. Hirayama, talk in the calorimeter session of this Workshop.

[11] E. Eichten, I. Hinchliffe, K. Lane, and C. Quigg, Rev. Mod. Phys. 56 (1984) 579.